International Journal of Applied Earth Observation and Geoinformation 149 (2026) 105302

Contents lists available at ScienceDirect

International Journal of Applied Earth Observation and Geoinformation

journal homepage: www.elsevier.com/locate/jag

Improving SPM retrieval across diverse transitional waters through satellite-derived OWT classification and per-class algorithm optimization

Junfang Lin [a,*], Elizabeth C. Atwood [a], Xiaohan Liu [a], Emmanuel Nwokocha [a], Thomas Jackson [b], Steve Groom [a]

[a] Plymouth Marine Laboratory, Prospect Place, The Hoe, Plymouth PL1 3DH, UK
[b] EUMETSAT, Eumetsat Allee 1, 64295 Darmstadt, Germany

ARTICLE INFO

Keywords:
Remote sensing
Suspended particulate matter
Optical Water type
Blending
Transitional water quality

ABSTRACT

Satellite remote sensing provides synoptic coverage and frequent revisit capabilities, making it an essential tool for estimating suspended particulate matter (SPM) in optically complex aquatic environments. Recent advances in satellite-derived optical water type (OWT) classification offer new opportunities for improving SPM retrieval across diverse water bodies, yet a systematic per-OWT recalibration and comparative evaluation of existing SPM algorithms has not been fully assessed. In this study, we employ a comprehensive framework that recalibrates 17 widely used SPM algorithms for each of 11 satellite-derived OWT classes and uses a Round-Robin evaluation to identify the optimal algorithm for each class while minimizing cross-type performance variability. Using Sentinel-2 MultiSpectral Instrument (MSI) reflectance, the resulting OWT-based blending scheme achieves substantially improved accuracy across optically diverse transitional waters, with a Root Mean Square Error (Ψ) of ~4.6–8.2 g/m^3 and a coefficient of determination (r^2) of 0.87–0.91 when validated against in-situ observations, including measurements from regions not used for calibration. The framework is further demonstrated through spatial mapping and multi-year trend analysis of SPM in two transitional coastal systems. The results highlight the value of satellite-derived OWTs for enhancing the transferability and robustness of SPM retrievals and provide a scalable approach for water-quality monitoring and ecosystem-assessment applications.

1. Introduction

Suspended particulate matter (SPM) in coastal and inland waters is influenced by a complex interplay of factors, including riverine discharge, anthropogenic dredging, natural sediment resuspension, and the hydrodynamic forces of tidal currents (Manivanan, 2008; Sent et al., 2025; Wolanski and Elliott, 2015). Elevated SPM concentrations impose significant impacts on aquatic ecosystems. Beyond diminishing water clarity and quality, high SPM levels strongly affect light attenuation, photosynthetic potential, the depth of the euphotic zone and trophic dynamics (Turner and Millward, 2002). Systematic and continuous monitoring of SPM variability is thus critical in supporting the preservation of ecological integrity and long-term sustainability of aquatic ecosystems, especially in optically complex environments.

Satellite and airborne remote sensing technologies have become indispensable for mapping SPM distributions, offering holistic and scalable insights into its spatial and temporal variability (Matthews, 2011; Odermatt et al., 2012). Over the years, advancements in satellite technology have significantly refined the precision (e.g., resolution) and expanded the capabilities of SPM retrieval, fostering the development of numerous algorithms tailored to different radiometric datasets and water conditions. These algorithms, broadly categorized into semi-analytical and empirical approaches, have been instrumental in advancing our understanding of SPM dynamics.

Semi-analytical algorithms are fundamentally based on radiative transfer theory, using the inherent optical properties (IOPs) of water to establish relationships with SPM concentrations. A key IOP within these algorithms, particle backscattering (b_{bp}), has been extensively validated as a reliable proxy for SPM concentration, as demonstrated in studies such as Neukermans et al. (2012) and Tavora et al. (2020). Conversely, empirical algorithms take a pragmatic approach, directly correlating spectral reflectance data with SPM concentrations, bypassing the complexity of IOP analysis. For example, the linear model by Jorgensen (1999) as well as the approaches by Nechad et al. (2010) and Ondrusek

* Corresponding author.
E-mail address: Junl@pml.ac.uk (J. Lin).

https://doi.org/10.1016/j.jag.2026.105302
Received 11 December 2025; Received in revised form 2 April 2026; Accepted 18 April 2026
Available online 30 April 2026
1569-8432/© 2026 The Authors. Published by Elsevier B.V. This is an open access article under the CC BY license (http://creativecommons.org/licenses/by/4.0/).

et al. (2012) have significantly enriched the field. Notably, studies like that of Doxaran et al. (2002) demonstrate how certain band ratios of remote sensing reflectance (R_{rs}) can be effective proxies for SPM concentration in specific environments.

Despite these advancements, both semi-analytical and empirical algorithms still face challenges in terms of versatility. While many were developed using data from specific regions, ensuring optimal results within those confines, their applicability often diminishes when extended beyond their origin. This limitation arises from the inherent variability in the optical properties of different water bodies, which can vary temporally due to factors such as riverine influxes and algal proliferation. These fluctuations, influenced by various environmental dynamics, can significantly affect the algorithm's accuracy. Moreover, the limitations are often rooted in assumptions underlying their developments. For instance, algorithms that rely on near-infrared (NIR) reflectance assume that this spectral band reliably captures SPM signals. While this is valid in turbid waters with high particulate concentrations, the NIR signal becomes negligible in clearer waters, leading to inaccurate or unusable estimates. Such context-specific assumptions constrain the adaptability of these algorithms across diverse aquatic environments.

To overcome these challenges, researchers have developed algorithms based on Optical Water Types (OWTs) to enhance inversion accuracy from remote sensing (Jiang et al., 2021; Moore et al., 2001; Novoa et al., 2017; Uudeberg et al., 2019). The approaches aim to group waters with similar optical properties and develop the optimal algorithm tuned for each OWT class. In principle, OWT-based algorithms are independent of geographic location and time, exhibiting less geographic specificity than traditional regional algorithms. However, broader utility is still limited by shortcomings in both the OWT classification and the SPM estimation algorithms currently employed. OWT classes used for water quality parameter estimation within the Ocean Colour Climate Change Initiative (OC-CCI) products were first built using in-situ reflectance data (Moore et al., 2009). In a subsequent iteration of OC-CCI, OWTs were updated to instead be based on satellite reflectance data with more comprehensive coverage in both space and time, as this provided a more balanced and representative training dataset (Jackson et al., 2017). OWT classes for freshwater and coastal systems have been developed based on in-situ reflectance data (Spyrakos et al., 2018) and have been demonstrated to greatly improve water quality parameter estimates when algorithms are calibrated on a per-OWT basis (Neil et al., 2019). Similar to developments within OC-CCI, questions arise as to the sufficient representativeness of an in-situ training dataset as compared to that from satellite with its more comprehensive coverage. Recent innovations, such as the pan-regional classification employed by Atwood et al. (2024), have showcased promising performance in OWT classification for transitional water systems based on satellite remote sensing reflectance data. A per-OWT algorithm calibration on an OWT set built from satellite reflectance data has to date not been performed. This progress can further accelerate efforts to refine SPM estimation methods grounded in OWT principles, potentially leading to more accurate SPM estimates particularly for transitional water systems. Building on these developments, a remaining challenge concerns the transferability of SPM algorithms across diverse optical environments. A key motivation for this study is that most previous OWT-based approaches used OWT classes derived from limited in-situ reflectance observations, which are often geographically biased and do not fully represent the optical diversity of transitional waters. The satellite-derived OWTs employed here provide substantially broader spatial and temporal coverage, enabling a more representative characterization of water types. Importantly, although OWTs have been applied, for example, to guide chlorophyll-a retrievals (Liu et al., 2021; Neil et al., 2019) in large-scale ocean-colour products, a systematic per-OWT recalibration and comparative evaluation of major SPM algorithms using satellite-derived OWTs has not yet been comprehensively assessed. This gap limits the transferability of existing SPM algorithms across diverse optical regimes, particularly in highly dynamic coastal waters.

Although SPM can often be retrieved reliably within individual regions, our analysis and previous studies show that the performance of any single algorithm varies substantially across different OWTs. This cross-type variability becomes a major source of uncertainty when applying regional algorithms to optically diverse waters, leading to inconsistent retrieval quality under both low and high turbidity conditions. Addressing this practical limitation requires an approach that explicitly accounts for the optical heterogeneity of water bodies. By recalibrating and selecting algorithms on a per-OWT basis, the present study aims to reduce this cross-type variability and provide more stable, transferable SPM retrievals across distinct aquatic environments.

This study pursues four primary objectives. First, we aim to perform a comprehensive assessment of major existing SPM retrieval algorithms, employing an independent matchup dataset including in-situ SPM measurements and Sentinel-2 MultiSpectral Instrument (MSI) reflectance (ρ_w) data. Second, building on the new OWT classification proposed by Atwood et al. (2024), the 17 candidate SPM algorithms are first recalibrated for each of the 11 OWTs, after which a Round-Robin assessment is conducted to determine the optimal algorithm for each OWT. Third, we apply an OWT-based blending approach for estimating SPM from MSI data and validate its accuracy using in-situ SPM measurements. Lastly, our study demonstrates the practical applicability of the proposed SPM blending approach, showcasing its effectiveness in estimating SPM levels within two coastal waters. An additional methodological contribution of this work is the introduction of a Round-Robin evaluation strategy to quantify the stability of each algorithm across spatially independent subsets. Unlike random data splits, which risk leakage between calibration and validation samples, the Round-Robin approach allows performance to be assessed under varied optical and regional conditions. This design provides a more rigorous test of generalizability and ensures that the algorithm selected for each OWT class performs consistently beyond the regions used for recalibration.

2. Data

An extensive dataset of in-situ SPM measurements was compiled in this study. The measurement locations include seven regions: the Elbe, Curonian, Tagus, Venice, Danube, Black Sea, and Étang de Berre (Fig. 1 and Table 1). The SPM concentrations were determined using the gravimetric method following established protocols (Strickland and Parsons, 1972). Water samples were collected from the field, transported to the laboratory, and filtered through 47 mm GF/F filters. The filtration volume was determined by starting with a small amount and incrementally increasing the volume until filtration slowed markedly, with adjustments made for differences in sediment load. Sample volumes typically ranged from 50 mL to 1,000 mL, depending on water clarity. The filters were then dried at 60°C for 24 h before weighing. By comparing the mass of the dried filter with and without the collected particles, and considering the volume of filtered water, the SPM concentration was calculated. These SPM measurements span a broad range, from ~ 0.3 to ~ 250 g/m^3 (Table 2 summarizes OWT-stratified SPM statistics). The dataset is representative of diverse aquatic environments, covering a wide optical range within transitional and coastal waters, including relatively clear offshore-adjacent waters.

MSI Level-1C imagery was atmospherically corrected using two complementary processors: POLYMER (v4.16; CERTO "minabs2" configuration) and ACOLITE (Generic version 20231023) operated in Dark Spectrum Fitting (DSF) mode (Vanhellemont and Ruddick, 2018). Processing was performed at 60 m spatial resolution. A common IdePIX cloud mask was applied to both products (MSI flags: IDEPIX_CLOUD, IDEPIX_INVALID, IDEPIX_CLOUD_AMBIGUOUS, IDEPIX_CLOUD_BUFFER, IDEPIX_VEG_RISK, IDEPIX_CLOUD_SHADOW, IDEPIX_SNOW_ICE, IDEPIX_MOUNTAIN_SHADOW, IDEPIX_CIRRUS_SURE). For POLYMER, valid water pixels additionally satisfied the standard

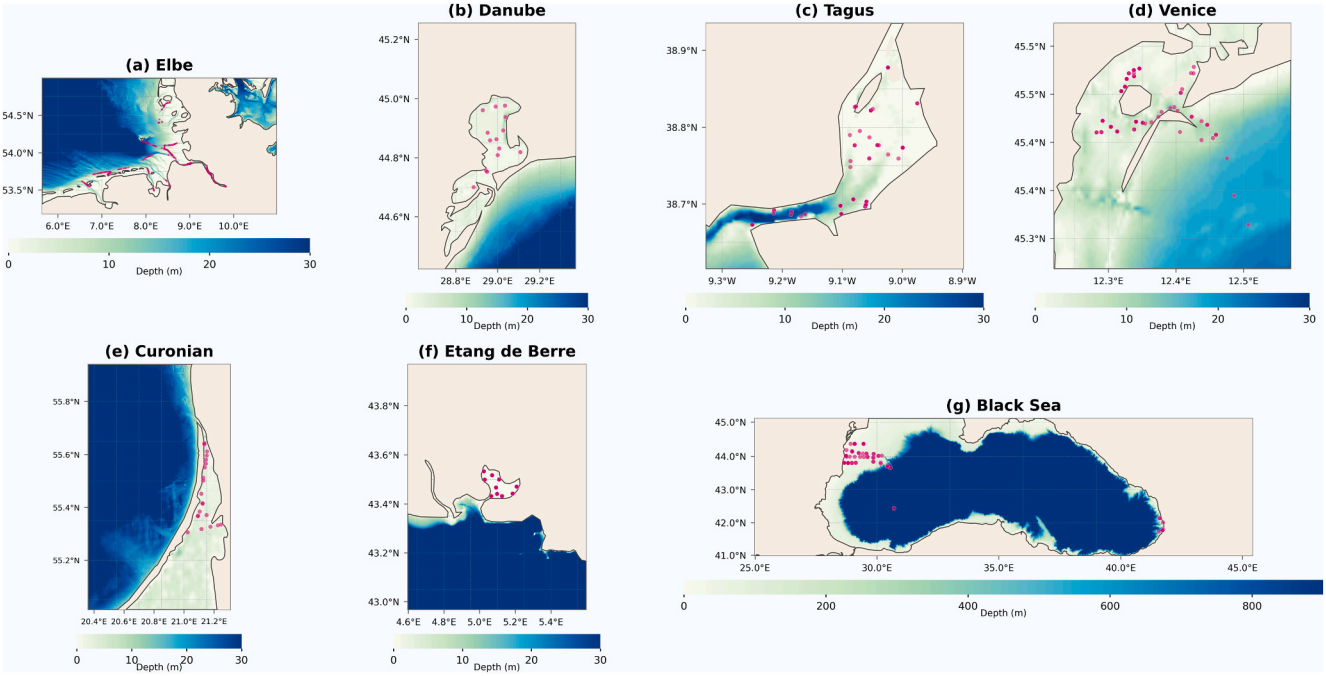

Fig. 1. Spatial distribution of in-situ SPM samples used for Sentinel-2 MSI matchups in the study regions. Magenta markers denote valid matchups between satellite and in-situ observations. Background colour indicates water depth (m). Panels show (a) Elbe, (b) Danube, (c) Tagus, (d) Venice, (e) Curonian, (f) Étang de Berre, and (g) Black Sea; the corresponding latitude/longitude bounds, sampling time ranges, and matchup counts are summarized in Table 1. To support model development and independent evaluation, matchups from Elbe and Danube were randomly split into Dataset A (calibration and Round-Robin assessment) and Dataset B (internal validation) using a 2:1 ratio, while matchups from Tagus, Venice, Curonian, Étang de Berre, and Black Sea were grouped into Dataset C for geographically independent validation (see Table 1 for region-wise counts and date ranges). (For interpretation of the references to colour in this figure legend, the reader is referred to the web version of this article.)

Table 1
In-situ monitoring coverage and sampling dates by region.

Region	Latitude (°)	Longitude (°)	Start Date	End Date	N
Elbe	53.49 – 54.70	6.54 – 10.06	2018–10-17	2021–06-28	1081
Danube	44.70 – 44.98	28.88 – 29.11	2021–04-22	2022–05-22	14
Tagus	38.67 – 38.88	−9.25 – -8.98	2017–12-09	2022–09-21	75
Venice	45.31 – 45.48	12.28 – 12.51	2021–03-05	2022–09-27	69
Curonian	55.31 – 55.64	21.02 – 21.25	2020–09-29	2022–11-06	21
Black Sea	41.72 – 44.36	28.65 – 41.74	2023–05-01	2024–06-17	62
Étang de Berre	43.40 – 43.53	5.02 – 5.21	2016–09-01	2019–07-24	129

Table 2
Number of matchups per OWT, with turbidity represented by in-situ SPM.

OWT	N	Median SPM (g/m^3)	Minimum SPM (g/m^3)	Maximum SPM (g/m^3)
1	43	0.84	0.36	0.98
2	45	1.12	0.39	3.80
3	60	1.47	0.37	8.86
4	230	3.41	0.28	13.65
5	90	2.79	0.89	7.40
6	147	3.63	0.35	32.20
7	210	4.51	2.03	31.16
8	249	11.13	4.03	43.95
9	138	20.17	4.70	250.0
10	50	23.25	6.77	212.24
11	189	54.27	30.14	98.54

POLYMER validity expression (bitmask & 10230) and $\rho_w < 0.12$ at all spectral bands. ACOLITE outputs were further masked for sun glint using $\rho_{gli} < 0.01$, where ρ_{gli} is the glint reflectance predicted from wind speed using the Cox and Munk (1954) model as implemented in POLYMER.

The final water-leaving reflectance $\rho_w(\lambda)$ was generated by per-band, pixel-wise merging of POLYMER and ACOLITE following the CERTO protocol (https://certo-project.org/Resources/CERTO_D5.4_final.pdf), using $\rho_{w,poly}(865)$ as the blending index:

$$\rho_w(\lambda) = \alpha\,\rho_{w,poly}(\lambda) + (1-\alpha)\,\rho_{w,aco}(\lambda), \tag{1}$$

with transition thresholds $\rho_{min} = 0.005$ and $\rho_{max} = 0.015$:

$$\alpha = \begin{cases} 1, & \rho_{w,poly}(865) < \rho_{min} \\ 0, & \rho_{w,poly}(865) > \rho_{max} \\ \dfrac{\rho_{max} - \rho_{w,poly}(865)}{\rho_{max} - \rho_{min}}, & \text{otherwise.} \end{cases} \tag{2}$$

Pixels in the transition zone ($0 < \alpha < 1$) were required to satisfy both POLYMER and ACOLITE quality masks. This formulation ensures a smooth transition between atmospheric-correction outputs across turbidity regimes while maintaining consistent quality control.

A procedure was implemented to obtain matchups of MSI-derived ρ_w data corresponding to each in-situ SPM measurement, resulting in a total of 1451 matchups. Satellite matchup statistics were derived using a 9-nearest-neighbour approach, which includes:

- Reflectance values for the centre pixel (the pixel closest to the sampling point).
- Descriptive statistics (mean, median, and standard deviation) for the 9 surrounding pixels.
- The number of valid pixels within the 9-nearest-neighbour set.

- The time difference between in-situ sampling and the satellite overpass.

The mean and standard deviation of the nearest-neighbour pixels were used to calculate the coefficient of variation for the matchup macro-pixel. The filtering criteria for matchups included three key factors: (1) the coefficient of variation is less than 0.2, (2) the number of valid pixels should be more than 5, and (3) the time difference between in-situ sampling and the satellite overpass should be no longer than 3 h. Fig. 1 presents a map illustrating the distribution of the sampling and matchup locations. Further, the water type classification methodology of Atwood et al. (2024) was employed to identify the dominant OWT associated with each matchup. The corresponding OWT membership scores were also recorded for subsequent SPM blending processing.

To facilitate a comprehensive and structured assessment of the proposed algorithms, the dataset was divided into three distinct subsets. Because Elbe and Danube include extensive temporal and spatial coverage, random splits were applied only within these regions to preserve independent observation conditions and reduce autocorrelation. Measurements from the Elbe and Danube regions were randomly split in a 2:1 ratio into Dataset A (730 points) and Dataset B (365 points). Dataset A was used for algorithm recalibration and evaluation, while Dataset B served as an internal evaluation set to examine interpolation performance within the same regional context. The 2:1 split was chosen to ensure adequate calibration sample size within each OWT class for stable per-OWT optimization while preserving an independent internal validation subset. We repeated the full workflow using alternative split ratios (70/30 and 80/20). The blended-product performance on Datasets B and C showed similar patterns across splits (Table S1).

To further assess the generalizability of the algorithm across different geographical regions, a third subset, Dataset C (356 points), was constructed using all measurements from the Tagus, Venice, Curonian, Black Sea, and Étang de Berre regions (Table 1). The Black Sea measurements were obtained from three research cruises and are publicly available via Zenodo (DOIs: https://doi.org/10.5281/zenodo.15120079; https://doi.org/10.5281/zenodo.15119521; https://doi.org/10.5281/zenodo.14978829). Dataset C was completely excluded from the algorithm recalibration process and used solely for independent evaluation. This region-based separation ensures that the assessment of the algorithm's transferability is conducted under conditions not represented in the calibration phase, thus providing a more robust estimate of performance on ecologically distinct regions.

3. Methods

3.1. SPM algorithms

A total of 17 SPM algorithms were selected and evaluated as part of this study. The selection covers the most widely used semi-analytical and empirical SPM algorithms across coastal and inland waters, capturing a wide variety of spectral relationships between reflectance and SPM. These algorithms are indicated by the lead author's name and the respective publication year: Jorgensen1999 (Jorgensen, 1999), Dekker1993 (Dekker, 1993), Nechad2010 (Nechad et al., 2010), Doxaran2002 (Doxaran et al., 2002), Yu2019 (Yu et al., 2019), Wei2021 (Wei et al., 2021), Novoa2017 (Novoa et al., 2017), Jiang2021 (Jiang et al., 2021), Siswanto2011 (Siswanto et al., 2011), Miller2004 (Miller and McKee, 2004), Ondrusek2012 (Ondrusek et al., 2012), Petus2010 (Petus et al., 2010), Balasubramanian2020 (Balasubramanian et al., 2020), Zhang2014 (Zhang et al., 2014), Vantrepotte2011 (Vantrepotte et al., 2011), Binding2010 (Binding et al., 2010) and BinUstir (Binding et al., 2010). In Section A of the Supplementary Materials, we present an overview of these 17 SPM algorithms. Some algorithms were implemented in multiple band/variant forms (e.g., different wavelengths), resulting in 22 model variants in total. The section summarizes their distinctive features, methodological approaches, and any noteworthy considerations associated with each algorithm. By comparing these algorithms, we aim to gain valuable insights into their capabilities and potential applications in estimating SPM for different water types.

3.2. Round-Robin assessment

The assessment of the algorithm's performance follows a methodology that incorporates univariate statistical tests typically employed for comparing modelled data with in-situ measurements. The statistics involved in the methodology include Pearson correlation coefficient (r), Root Mean Square Error (Ψ), Bias (δ), Centre-pattern Root Mean Square Error (Δ), Slope (S) and intercept (I) of a Type-2 regression, and Percentage of possible retrievals (η). The definitions of these statistics can be found in Section B of Supplementary Materials. Each metric is evaluated individually, and a scoring system is employed to determine each algorithm (or model) performance. Finally, a procedure of bootstrapping and multi-metric scoring is performed. While this approach builds on the methodology outlined in Brewin et al. (2015), a key distinction is that we compare against the best model performance rather than the mean performance. We use 10,000 bootstrap resamples to obtain stable score distributions. More details can be found in Section B of Supplementary Materials.

3.3. OWT classification

Building upon the Ocean Colour Climate Change Initiative (OC-CCI) and the Lakes Climate Change Initiative (Lakes_cci), Atwood et al. (2024) have presented a refined and enhanced method for classifying OWTs to accurately identify transition zones between fresh- and saltwater provinces. This innovative approach utilizes advanced fuzzy clustering methods to generate OWT classes from satellite remote sensing products, effectively grouping together spectrally distinct water bodies observed over the analyzed space/time period. There are a total of 11 OWTs involved in the analysis (Table 2). The 11-class system represents the optimal cluster solution achieved following the method by Atwood et al. (2024) for transitional waters. Each pixel will be assigned 11 membership values, one for each OWT. The dominant OWT classification for a given pixel will be determined by selecting the OWT with the highest membership value among the 11 assigned values.

To ensure that the OWT assignment is suitable for subsequent algorithm selection and membership-weighted blending, we performed a brief quality assessment of the fuzzy memberships. Because the OWT product provides continuous per-pixel membership vectors across 11 classes rather than supervised discrete labels, we evaluated OWT reliability using (i) membership-structure diagnostics and (ii) physical-consistency checks based on the matchup dataset. Membership structure was summarized by the top-3 membership sum $S_3 = m_1 + m_2 + m_3$ (three largest memberships for each matchup/pixel) and the membership difference $D = m_1 - m_2$, where small D indicates optically mixed/transitional spectra. Physical consistency was assessed by comparing in-situ SPM among dominant OWT classes (Kruskal–Wallis with post-hoc tests), supporting that OWT memberships separate optical regimes relevant to SPM retrieval. Because transitional/mixed pixels are common, we blend SPM estimates using normalized top-3 memberships to improve stability at class boundaries. These diagnostics are provided in Supplementary Fig. S1.

3.4. SPM blending

Following Liu et al. (2021), we implemented a fuzzy-membership weighted blending procedure based on the OWT membership values to generate a continuous SPM product and reduce cross-OWT variability. For each OWT class $k \in \{1, \cdots, 11\}$, a single best-performing SPM algorithm $f_k(\cdot)$ was identified from the Round-Robin assessment (Section 3.2) and recalibrated for that OWT (Section 3.5; Table 3). For a given pixel, the OWT classifier provides membership values m_k for all 11

Table 3
Lookup table with optimal SPM algorithms for each OWT.

OWT	Optimal algorithm	Parameter	Wavelength (λ_0, λ_1,.. λ_n)	Recalibrated coefficients
1	Siswanto2011	$c_{0\text{-}2}$	490, 560, 665	1.27, 25.62, −2.19
2	Nechad2010	A^ρ, C^ρ	783	1798.7, 0.12
3	Jorgensen1999	m, n	560	14.27, −4.97
4	Wei2021	$c_{0\text{-}3}$, $a_{0\text{-}1}$, $b_{0\text{-}2}$	443, 490, 560, 665, 740, 865	0.26, 0.27, 1.15, 0.10, 20.41, 2.16, 0.48, 1.06, 0.43
5	Siswanto2011	$c_{0\text{-}2}$	490, 560, 665	1.21, 9.78, −0.80
6	Nechad2010	A^ρ, C^ρ	783	1542.33, 2.05
7	Nechad2010	A^ρ, C^ρ	783	1074.83, 2.16
8	Wei2021	$c_{0\text{-}3}$, $a_{0\text{-}1}$, $b_{0\text{-}2}$	443, 490, 560, 665, 740, 865	0.38, 0.01, 4.01, 0.12, 20.42, 2.21, 0.52, 1.02, 0.45
9	Wei2021	$c_{0\text{-}3}$, $a_{0\text{-}1}$, $b_{0\text{-}2}$	443, 490, 560, 665,740, 865	0.52, 0.01, 0.56, 0.16, 20.52, 2.13, 0.47, 1.03, 0.48
10	Miller2004	c_0, c_1	665	1512.09, 0.17
11	Wei2021	$c_{0\text{-}3}$, $a_{0\text{-}1}$, $b_{0\text{-}2}$	443, 490, 560, 665, 740, 865	0.41, 0.92, 2.49, 0.10, 20.50, 2.12, 0.50, 1.01, 0.46

classes (Section 3.3). We selected the three largest memberships and denote their indices by $\mathscr{K}$(top-3 OWTs). For each $k \in \mathscr{K}$, an OWT-specific SPM estimate ($\widehat{C}_k$) was computed as

$$\widehat{C}_k = f_k(\rho_w(\lambda)), \tag{3}$$

where $\rho_w(\lambda)$ is the MSI water-leaving reflectance at the required bands. The final blended SPM estimate was obtained by membership-weighted averaging across the top-3 OWTs:

$$\widehat{C} = \sum_{k\in\mathscr{K}} w_k \widehat{C}_k, \text{with } w_k = \frac{m_k}{\sum_{j\in\mathscr{K}} m_j}. \tag{4}$$

Here, the weights w_k are normalized per pixel such that $\sum_{k\in\mathscr{K}} w_k = 1$. We focused on the top-3 blending strategy because it provided the best trade-off between stability and sensitivity in cross-OWT tests, while preliminary tests using fewer memberships (top-2) or all memberships yielded less consistent performance.

3.5. Algorithm recalibration

To improve the precision of SPM algorithms for each OWT class, we performed a recalibration of their coefficients. This recalibration process relied on the integration of MSI ρ_w matchups and in-situ SPM measurements. To achieve this, we employed a global optimization routine from the SciPy Python package (*scipy.optimize*). The cost function employed for this recalibration is defined as follows:

$$Fun_{cost} = \left[\frac{1}{n}\sum_{i=1}^{n}\left(\frac{\log\left[C^S_{spm}(i)\right] - \log\left[C^I_{spm}(i)\right]}{\log\left[C^I_{spm}(i)\right]} \bullet W_{OWT}(i)\right)^2\right]^{0.5} \tag{5}$$

where C^S_{spm} and C^I_{spm} are satellite-derived and in-situ SPM, respectively; $W_{OWT}(i)$ is the optimization weight, set to membership $m_k(i)$ for recalibration within OWT k and to 1 for the global (non-OWT-stratified) recalibration; and n is the number of matchups. A log-relative formulation was chosen because SPM spans ~ two orders of magnitude, making relative log-errors more stable than absolute errors.

4. Results

4.1. Round-Robin assessment of optimal algorithms recalibrated for each OWT

Prior to implementing the blending process, it is essential to identify the optimal algorithm for each OWT. To support this selection, a Round-Robin assessment was conducted using Dataset A. This procedure involved evaluating the performance of 17 distinct SPM algorithms (22 SPM models in total), each recalibrated for individual OWTs using Eq. (5). Performance scores, ranging from 0 to 1, were assigned based on the scoring methodology detailed in Section B of Supplementary Materials.

Fig. 2 illustrates the distribution of performance scores for the candidate algorithms applied to OWT7, presented here as a representative example. The scores range from approximately 0.4 to 1.0, with the Nechad2010 algorithm at 783 nm achieving the highest score of 1.0. Fig. 3 further compares SPM estimates derived from MSI data with in-situ SPM concentrations for OWT7, confirming that the Nechad2010 algorithm at 783 nm provides the most accurate results, with an r^2 of ~ 0.88 and a Ψ of ~ 7.3 g/m^3. The close alignment of scatter points along the 1:1 line further underscores the robustness of this retrieval.

A second example for OWT9 is presented in Figs. 4 and 5. In this case, the Wei2021 and Yu2019 algorithms achieved the highest performance scores, each producing Ψ values around 8.3 g/m^3. Notably, Wei2021 is an updated version of Yu2019 and retains a similar formulation for turbid waters; as such, the same set of coefficients was adopted for OWT9.

The optimal algorithm selected for each OWT is summarized in Table 3. Based on these results and following the blending framework described in Section 3.4, the optimal SPM estimates can be generated across OWT classes using MSI data in conjunction with the lookup table provided in Table 3.

4.2. Comparison of SPM algorithms

4.2.1. Comparison of recalibrated models and blending (Dataset A)

To evaluate the performance of the 17 SPM algorithms (22 models) and the proposed blending framework, we conducted a quantitative assessment using Dataset A. Each of the 22 SPM models was recalibrated using Eq. (5) with data from Dataset A, and the resulting coefficients are listed in Table 4. The blending algorithm was also tuned using the same dataset (Dataset A), with optimal model selection performed for each OWT based on the Round-Robin results described in Section 4.1.

Fig. 6 presents a comprehensive comparison of the retrieval accuracy across all models, including the blending approach in this study. The results show that several individual algorithms performed well after recalibration. For example, the Wei2021 and Yu2019 algorithms yielded strong agreement with in-situ SPM concentrations, achieving Ψ values of approximately 11.9 g/m^3 and r^2 values up to 0.79. These models effectively captured the general trends in the data, particularly at moderate and high SPM concentrations, but challenges remain, particularly in the lower concentration range (SPM < ~3 g/m^3), where a tendency toward overestimation is still evident.

A similar pattern is observed for the Nechad2010 algorithm at 783 nm, which achieved a Ψ of 12.9 g/m^3 and $r^2 = 0.82$. This behaviour is consistent with the design of the 783 nm band-based model, which is particularly sensitive to particle backscattering in moderately to highly turbid waters but becomes less informative when reflectance approaches saturation at very high SPM or falls close to the noise level at very low SPM. Some increase in dispersion was observed at both the low (<5 g/m^3) and high (>30 g/m^3) ends of the SPM range, suggesting reduced retrieval consistency under these conditions. Models such as Jorgensen1999 (Fig. 6a) and Doxaran2002A/B (Fig. 6h/i) exhibit relatively lower accuracy, with higher dispersion and bias.

Several existing SPM retrieval algorithms, such as Jiang2021 (Fig. 6l) and Novoa2017 (Fig. 6m), incorporate the use of other OWT classification to enhance estimation performance. However, in our evaluation, these OWT-based methods did not exhibit clear advantages over other individual algorithms. Their retrievals were characterized by substantial dispersion and relatively modest accuracy.

In contrast, the OWT-based blending algorithm in this study outperformed all other algorithms (Fig. 6w). By integrating the optimal

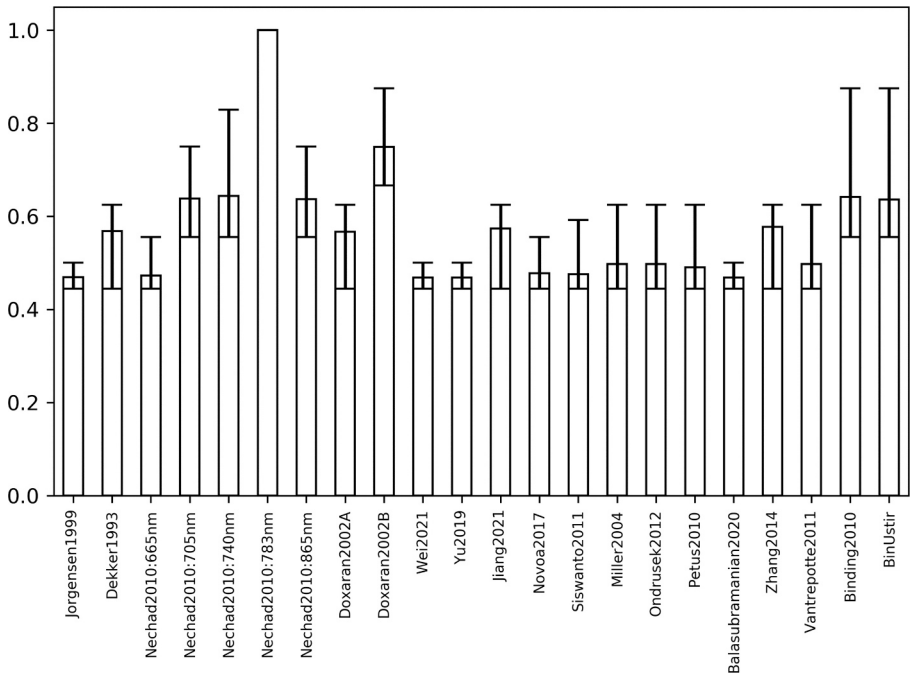

Fig. 2. Distribution of Round-Robin assessment scores (closer to 1 is top performing) for the 22 recalibrated SPM models, evaluated on the OWT7 subset of Dataset A.

algorithm for each OWT class, the blending framework achieved a markedly lower overall error ($\Psi = 6.9$ g/m^3) and the highest r^2 value (0.88). These results demonstrate that the blending approach not only preserves the strengths of the best-performing models but also mitigates their weaknesses by adapting to optical variability across water types.

4.2.2. Independent evaluation of SPM models using Dataset B

To further assess the capability of the recalibrated SPM models and the blending algorithm, an additional evaluation was conducted using Dataset B. This dataset consists of independent samples from the same regions as Dataset A, namely, the Elbe and Danube, but was entirely excluded from both the recalibration of the individual SPM algorithms and the tuning of the blending algorithm. As such, Dataset B provides a more robust validation scenario within the same geographic domain, allowing performance assessment under spatially and temporally independent conditions.

Fig. 7 presents the comparison between MSI-derived SPM estimates and in-situ measurements for Dataset B. Overall, the results corroborate the findings from Dataset A, demonstrating that many of the recalibrated models retain good performance when applied to previously unseen data from the same regions. For example, the Wei2021 and Nechad2010 (783 nm) models continue to yield high r^2 values (> 0.8) and relatively low Ψ values (~10–13 g/m^3), indicating stable retrieval behaviour across independent samples.

Importantly, the blending algorithm again outperforms individual models in this evaluation. It achieves the highest r^2 value (0.91) and the lowest Ψ (8.2 g/m^3), confirming its ability to generalize within the calibration domain while maintaining superior accuracy and consistency. The close alignment of scatter points with the 1:1 line and reduced bias across the SPM range further reinforce the robustness of the blending framework.

4.2.3. External validation using Dataset C

To evaluate the spatial transferability of the recalibrated SPM models and the blending algorithm, an independent validation was conducted using Dataset C, which comprises measurements from the Tagus, Venice, Curonian, Black Sea, and Étang de Berre regions. Unlike Datasets A and B, Dataset C originates from regions that were entirely excluded from both the algorithm recalibration and the blending model tuning process. As such, this evaluation provides a stringent test of the algorithms' ability to generalize to previously unseen geographic and optical conditions.

Fig. 8 presents the model evaluation results for Dataset C. Across most models, a decline in retrieval accuracy is observed compared to results from Datasets A and B, reflecting the challenges associated with transferring models to new environments. Part of this degradation likely reflects regional shifts in the ρ_w–SPM relationship across the independent validation sites, potentially associated with differences in particle composition and shallow-water/bottom effects (Martin et al., 2025). For example, Nechad2010 at 705 nm (Fig. 8d), Wei2021 (Fig. 8j), and Yu2019 (Fig. 8k) all exhibit a tendency to underestimate SPM across the entire concentration range, with r^2 values below 0.55 and a noticeable spread of points away from the 1:1 reference line. Several other models, including Dekker1993, Zhang2014, Novoa2017, and Ondrusek2012, also demonstrate weaker performance, characterized by higher bias and lower correlation with in-situ observations. These results highlight the challenge of directly transferring algorithms to new regions without recalibration, particularly in optically complex waters.

Despite these challenges, the blending algorithm again demonstrates superior performance when applied to Dataset C (Fig. 8w). It achieves the best overall retrieval accuracy, with the lowest Ψ of 4.6 g/m^3 and the highest r^2 of 0.87. Visual inspection confirms that the scatter points are more tightly clustered around the 1:1 line, indicating improved consistency across diverse water types.

These results underscore the advantage of the OWT-based blending approach in handling optical variability across regions. By dynamically adapting to the local water type and applying the most appropriate algorithm, the blending framework improves generalizability and retrieval robustness, even under previously unseen environmental conditions.

4.3. Application to satellite imagery

While the framework was applied across all study regions shown in Fig. 1, we present the Danube Delta–Razelm–Sinoe Lagoon Complex and the Tagus–Sado system as two representative case studies because they exhibit strong nearshore–offshore turbidity gradients and provide sufficient multi-year cloud-free Sentinel-2 coverage for demonstrating both

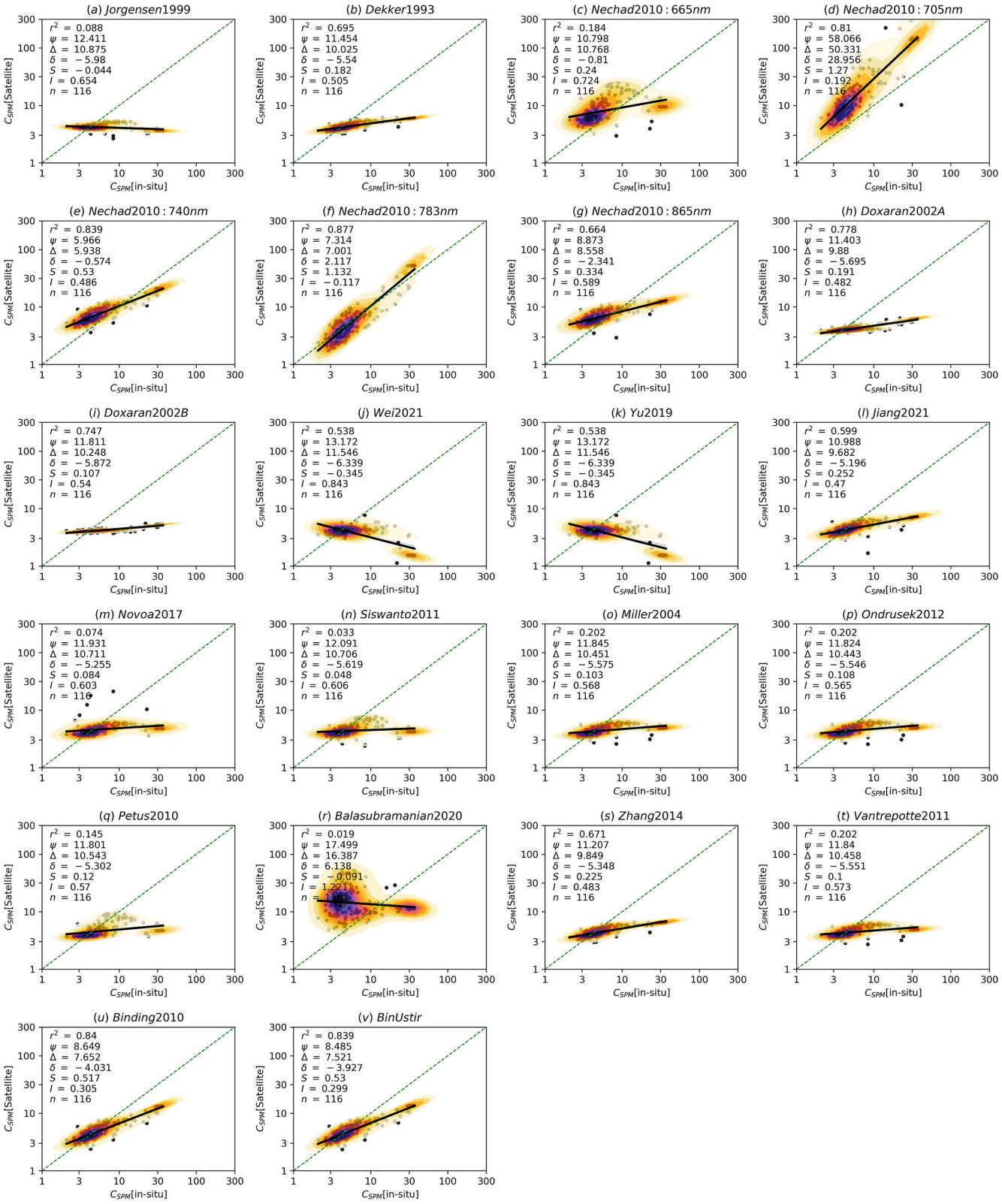

Fig. 3. Comparison of in-situ SPM concentrations with MSI-derived estimates across 22 models, using recalibrated coefficients from the OWT7 subset of Dataset A.

spatial mapping and temporal variability. Additional SPM and OWT maps for the remaining regions (Elbe, Venice, Curonian, Black Sea, and Étang de Berre) are provided in Supplementary Figs. S2–S6 using identical processing and visualization settings.

An application of the SPM blending method within the Danube Delta-Razelm-Sinoe Lagoon Complex coastal area in Romania is depicted in Fig. 9. The aquatic environment in this region is characterized by its complexity, with SPM concentrations spanning a wide range from ~ 0.1 to ~ 110 g/m^3. Notably, areas closer to the coastline and inland waters exhibit a prevalence of turbid pixels, primarily attributed to the influence of riverine inputs and bottom suspension processes (Fig. 9a). These areas are characterized by a dominant OWT, distinctly observed within

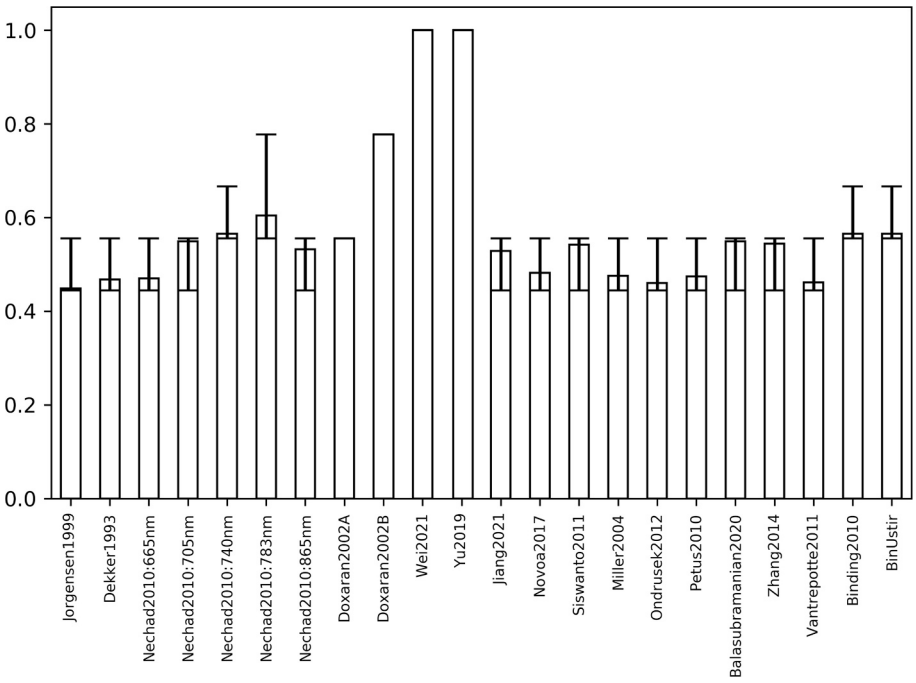

Fig. 4. Distribution of Round-Robin assessment scores for the 22 recalibrated SPM models, evaluated on the OWT9 subset of Dataset A (same format as Fig. 2).

the 7 to 11 range (Fig. 9b). In contrast, offshore waters in this locale exhibit remarkable clarity on that date, with SPM levels within the range of approximately 0.1 to 1 g/m^3. The prevailing OWT in these offshore areas tends to fall within the range of 1 to 2. An examination of the monthly time series data for SPM concentrations at the designated location (marked by a '+' in Fig. 9), as illustrated in Fig. 10a, reveals fluctuations ranging from ~ 4 to 20 g/m3, with an average concentration of ~ 11 g/m3. The highest SPM values tend to occur during the winter months, while the lowest values are recorded during the summer season. These temporal trends align with corresponding variations in the dominant OWT, characterized by a peak OWT of 10 in the winter and a mix of OWT 5 and 6 during the summer months.

Fig. 11 presents another application within the Tagus region in Portugal, showcasing the pronounced influence of two river estuaries on the distribution of SPM in the coastal area. As shown in Fig. 11a, inland waters heavily impacted by associated river systems of this region can exhibit substantially elevated SPM concentrations, peaking at ~ 80 g/m^3. However, as one approaches the estuary mouths, the SPM levels experience a gradual decline, settling at ~ 4 g/m^3, before further diminishing to ~ 0.1 g/m^3 in the offshore expanses. In Fig. 11b, we gain insight into the distribution of OWT within this area. Inland waters predominantly exhibit OWT within the range of 7 to 11, while the offshore regions are distinctly characterized by a dominant OWT range of 1 to 2. Additionally, Fig. 12 also provides insight into the SPM and OWT profiles along a transect extending from the Sado estuary mouth to the offshore region. Along this transect, we observe a sharp increase in SPM concentrations, rising from ~ 3 to ~ 8 g/m^3, followed by a gradual decline from ~ 8 to ~ 0.3 g/m^3 as we move further offshore. Simultaneously, the OWT undergoes a transition from OWT 8 to OWT 1 across this transect. It is noteworthy that a marked OWT transition at latitude 38.44°, over a distance of ~ 200 m, shows a shift from OWT 4 to OWT 1. Intriguingly, despite this OWT shift, the SPM concentrations remain relatively constant.

5. Discussion

5.1. Round-Robin assessment for OWTs

By quantifying scores within each OWT by Round-Robin assessment, a key finding is the strong performance alignment between certain algorithms and specific OWTs, such as Nechad2010 at 783 nm for OWT7, underscoring the necessity of selecting models that match the IOPs of each water type. This reflects the fact that the spectral shape and magnitude of satellite ρ_w—and therefore the relative influence of absorption and backscattering—vary strongly among OWTs, making certain algorithms inherently more compatible with specific optical regimes. The Round-Robin assessment systematically compares algorithms across OWTs, ensuring that selection is data-driven rather than subjective, which can be a crucial factor in environmental monitoring where accurate SPM estimates inform water quality assessments and ecosystem management.

Beyond optimizing algorithm selection, the Round-Robin approach highlights a fundamental limitation: algorithms calibrated for specific conditions often struggle in unfamiliar optical environments, emphasizing the need for adaptive models. These findings advocate for future algorithm development to prioritize flexibility and contextual adaptability, ensuring robust performance across diverse aquatic systems.

5.2. Recalibrated model performance and the role of the blending framework

The evaluation of 22 recalibrated SPM models and the proposed OWT-based blending algorithm across three independent datasets provides key insights into the strengths and limitations of current satellite-based SPM retrieval strategies. The results underscore the importance of context-specific recalibration and highlight the advantage of adaptive multi-model approaches in optically complex waters.

Using Dataset A, which served as the calibration dataset, many individual algorithms performed reasonably well after coefficient tuning, particularly under moderate to high SPM concentrations. However, systematic biases—such as overestimation at low SPM levels or underestimation in transitional ranges—were still evident across several

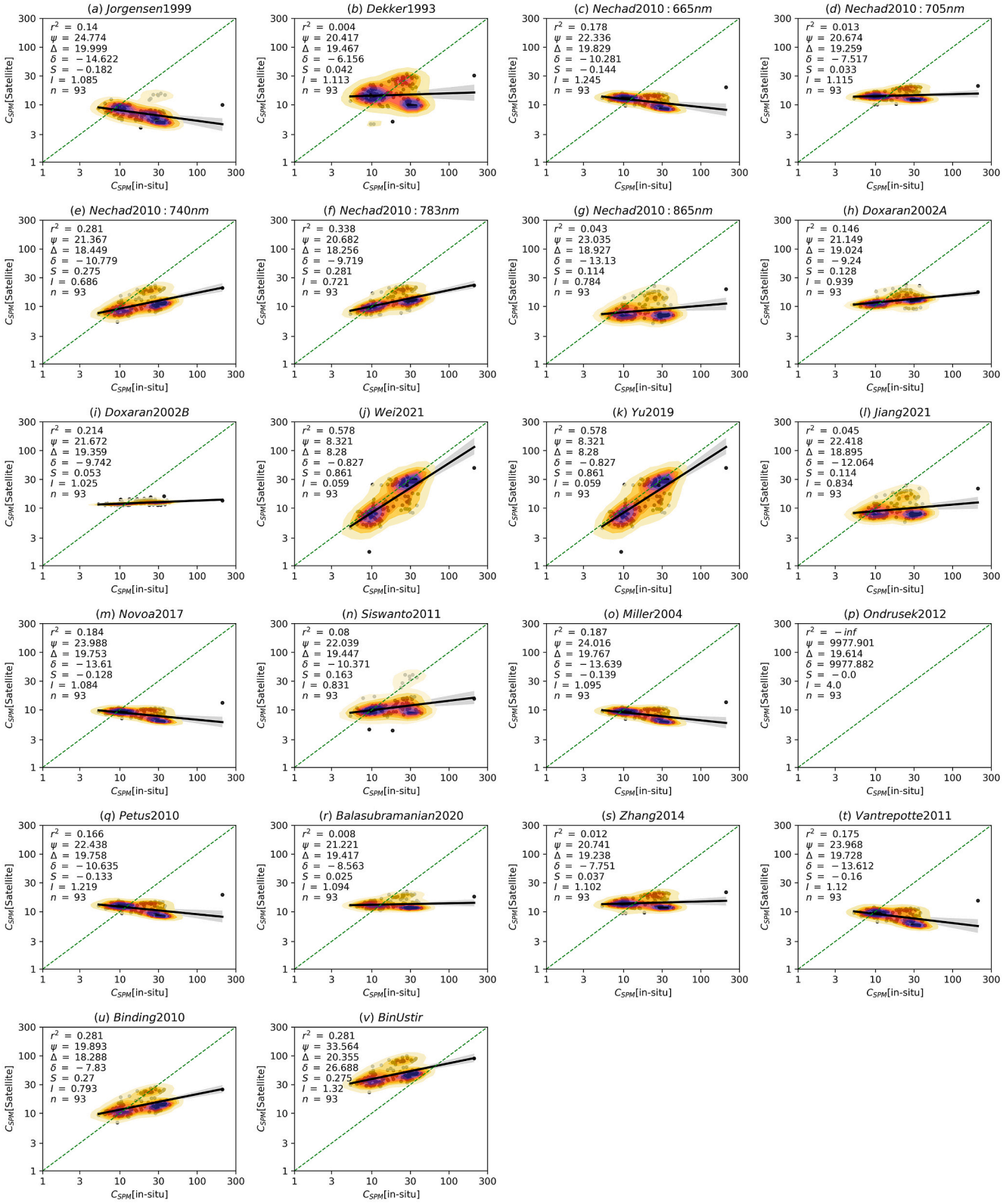

Fig. 5. Comparison of in-situ SPM concentrations with MSI-derived estimates across 22 models, using recalibrated coefficients from the OWT9 subset of Dataset A (same format as Fig. 3).

models. These patterns indicate that, while recalibration improves model alignment with local optical conditions, it does not universally resolve the challenges posed by spectral diversity in SPM–ρ_w relationships.

Evaluation using Dataset B, drawn from the same regions as Dataset A but withheld from recalibration, confirmed the internal consistency of the recalibrated models. Although originating from the same broader regions, Dataset B consisted of non-overlapping sampling times and locations, reducing the likelihood of autocorrelation or information leakage from the calibration set. Several algorithms retained robust

Table 4
Original and recalibrated coefficients of the SPM algorithms selected in this study.

Algorithm	Parameter	Wavelength (λ_0, λ_1,.. λ_n)	Original coefficients	Recalibrated coefficients
Jorgensen1999	m, n	560	269, 0.09	4.07, 0.001
Dekker1993	m, n	705	331, 2.69	1098.8, 0.15
Nechad2010	A^{ρ}, C^{ρ}	665	41.6, 0.19	253.7, 37.2
		705	77.0, 0.21	359.6, 46.4
		740	326.1, 0.12	1069.3, 198.8
		783	237.1, 0.15	875.5, 361.5
		865	488.6, 0.22	1449.6, 508.5
Doxaran2002A	m_0, m_1	865, 560	0.32, 0.96	33.8, 63.7
Doxaran2002B	n_0, n_1	865, 665	0.19, 0.48	1.42, 2.59
Yu2019	$c_{0\text{-}3}$, $a_{0\text{-}1}$	490, 560, 665, 740, 865	0.04, 1.17, 0.4, 14.86, 20.43, 2.15	0.15, 0.37, 4.58, 0.01, 20.51, 2.16
Wei2021	$c_{0\text{-}3}$, $a_{0\text{-}1}$, $b_{0\text{-}2}$	443, 490, 560, 665,740, 865	0.04, 1.17, 0.4, 14.86, 20.43, 2.15, 0.52, 0.93, 0.43	0.15, 0.37, 4.58, 0.01, 20.31, 2.12, 0.49, 1.03, 0.49
Novoa2017	g_0, r_0, n_0, n_1	560, 665, 865	96.6, 575.8, 32110, 2204	76.9, 247.6, 596.7, 352.1
Jiang2021	$c_{0\text{-}3}$	560, 665, 740, 865	94.6, 114.0, 137.7, 166.2	54.1, 58.8, 41.1, 47.1
Siswanto2011	$c_{0\text{-}2}$	490, 560, 665	0.65, 25.62, −0.65	1.21, 30.16, −1.68
Miller2004	c_0, c_1	665	1140.25, 1.91	1800.41, 2.67
Ondrusek2012	$c_{0\text{-}2}$	665	3.88, −13.8, 19.61	0.06, 1.24, 3.46
Petus2010	$c_{0\text{-}2}$	665	12450, 666.1, 0.48	38873, 643.8, 0.76
Balasubramanian2020	–	–	–	–
Zhang2014	c_0, c_1	705	362507, 2.32	110267, 1.97
Vantrepotte2011	A^{ρ}, C^{ρ}	665	1.092, 0.142	0.01, 0.17
Binding2010	b^*_{SPM}, b_b/b	740	0.554, 0.019	0.553, 0.033
BinUstir	b^*_{SPM}, b_b/b	740	0.664, 0.019	0.712, 0.018

performance, suggesting that spatial and temporal variability within a single region may be sufficiently captured by regional tuning. However, discrepancies remained in cases where model performance was less stable or consistent, revealing limitations in generalizing even within an otherwise familiar optical domain.

Dataset C provided the most rigorous test by evaluating performance in entirely novel geographic regions excluded from model development. Here, the degradation in performance among many recalibrated algorithms was pronounced, with increased bias and reduced correlation, especially in lower concentration regimes. These declines are consistent with well-known shifts in the ρ_w–SPM relationship arising from differences in sediment mineralogy and bottom influence across regions. These results highlight a critical limitation of conventional model transfer: algorithms calibrated for one region often fail to generalize across regions with distinct inherent optical properties and SPM dynamics.

In contrast, the blending algorithm consistently demonstrated superior performance across all three datasets. Its strength arises from exploiting cross-OWT diversity: rather than relying on a single parameterization of the ρ_w–SPM relationship, the blending approach adaptively selects algorithms whose empirical or semi-analytical structures best match the local optical conditions, thereby minimizing systematic biases across water types. By dynamically selecting the most suitable algorithm for each water type, the OWT-based blending framework mitigated the limitations of any single model and provided more stable and accurate retrievals across diverse environments. Notably, the blending approach maintained high retrieval accuracy not only within the calibration domain (Dataset A and B) but also under fully independent conditions (Dataset C), underscoring its potential as a scalable, transferable solution for operational SPM monitoring.

While OWT-based approaches have been explored for water-quality variables such as chlorophyll-a (Liu et al., 2021; Neil et al., 2019), systematic per-OWT recalibration and comparative evaluation of a large suite of SPM algorithms has received far less attention, particularly when using satellite-derived OWTs. Importantly, our approach leverages satellite-derived water type classification, enabling fully remote and adaptive algorithm integration. These findings reinforce the need for regionally flexible, multi-model strategies in aquatic remote sensing, particularly for variables like SPM that are governed by complex and spatially variable biogeochemical processes.

5.3. Sources of uncertainty and OWT-dependent error characteristics

5.3.1. Atmospheric correction (AC) uncertainty

Uncertainty in MSI water reflectance (ρ_w) remains a key error source for SPM retrieval in transitional waters, where adjacency effects, thin cloud/haze, sun glint, and spatially variable aerosols can bias both the magnitude and spectral shape of ρ_w. Because many SPM algorithms apply nonlinear transforms and/or band ratios, small residual reflectance errors can propagate into systematic SPM bias, particularly at low SPM where water-leaving signals approach the noise floor. In this study, we mitigate AC-related artifacts by blending POLYMER and ACOLITE outputs under CERTO-style pixel-level quality screening; nevertheless, residual AC uncertainty likely contributes to scene-to-scene variability and to dispersion in the lowest SPM regime.

5.3.2. OWT classification uncertainty and transitional pixels

The OWT product provides fuzzy memberships rather than hard labels, and classification ambiguity is expected at water-mass boundaries (e.g., plume edges). Pixels with low membership difference $D = m_1 - m_2$ (top-1 minus top-2 membership) represent transitional spectra where multiple OWTs are similarly plausible. In such cases, reliance on a single dominant class can introduce instability in per-pixel algorithm assignment and increase retrieval uncertainty. This directly motivates our top-3 membership blending strategy, which reduces sensitivity to boundary effects by allowing multiple optically plausible OWTs to contribute to the final estimate. Consistent with this rationale, the membership-structure diagnostics show that the top-3 memberships capture most of the membership mass (high S_3; Supplementary Fig. S1a), supporting the use of normalized top-3 membership blending. Moreover, the OWT-stratified validation metrics (Supplementary Fig. S7) demonstrate that retrieval errors and bias patterns vary substantially across OWTs, supporting the need for a fuzzy blending approach in optically heterogeneous waters.

5.3.3. Algorithm structural limitations

Even after recalibration, individual algorithms retain intrinsic structural constraints. NIR-based formulations can lose sensitivity in clear waters (signal-to-noise limitation) and may saturate at very high turbidity, while empirical band-ratio approaches can be sensitive to region-specific particle composition and bottom influence. These structural limitations explain why no single algorithm performs consistently across all OWTs, and why per-OWT selection combined

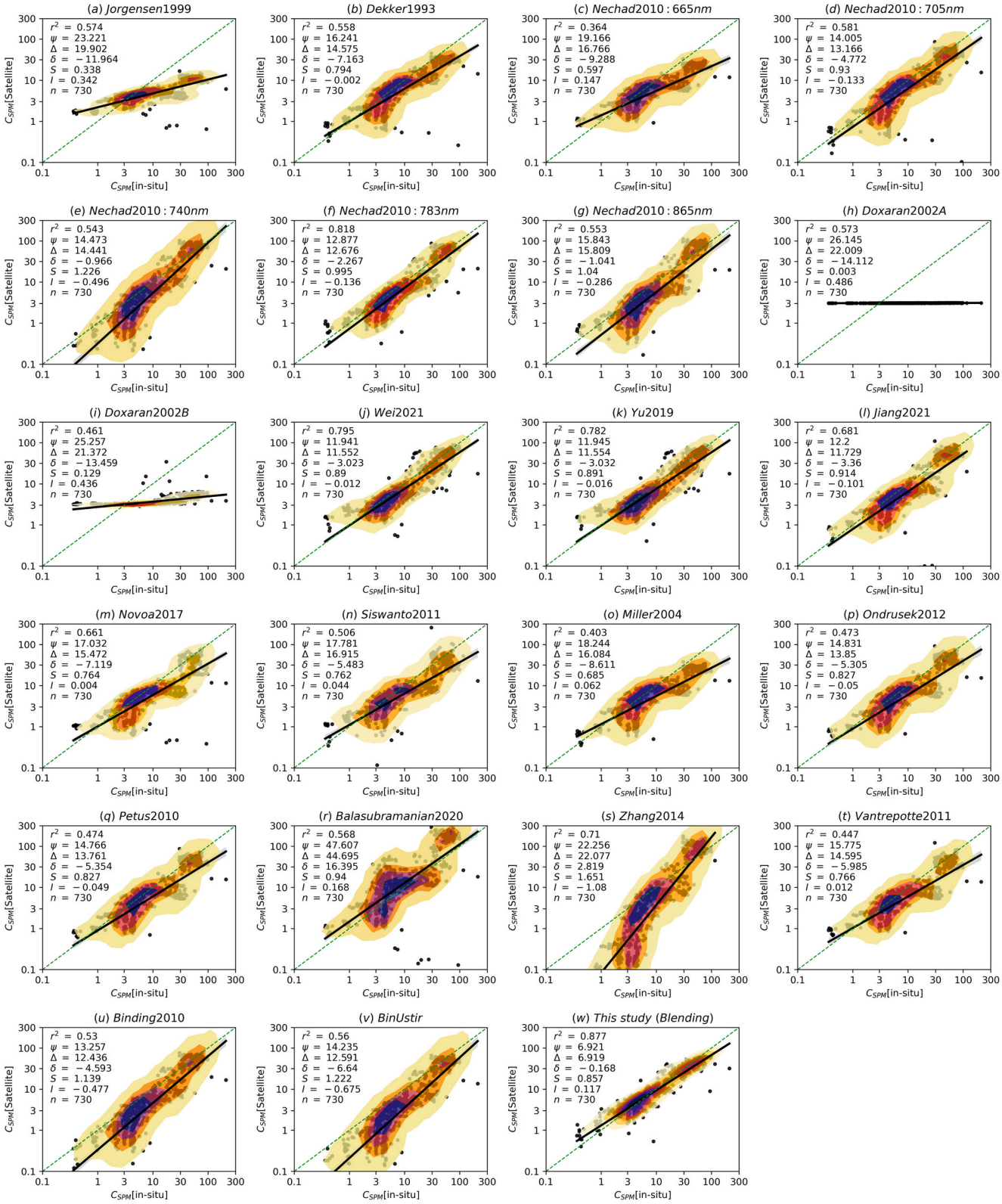

Fig. 6. Model performance on the calibration dataset (Dataset A). Scatterplots show MSI-derived SPM estimates versus in-situ observations for 22 recalibrated SPM models and the OWT-based blending algorithm (panel w), all evaluated on Dataset A. This dataset was used for both coefficient recalibration and blending optimization. Several models demonstrate good agreement with in-situ data, while the blending approach achieves the highest accuracy across the full range of optical conditions.

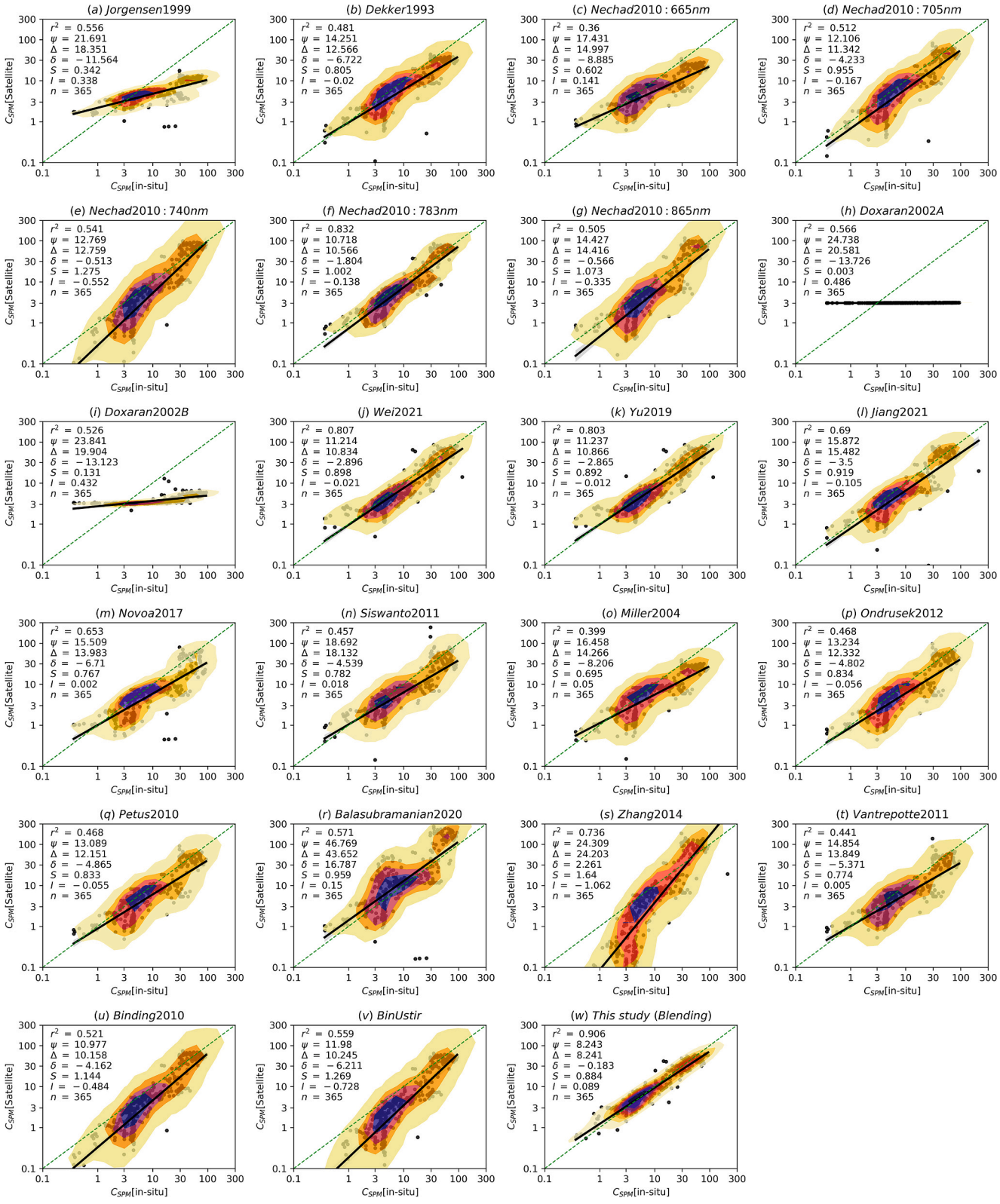

Fig. 7. Independent validation within the recalibration domain using Dataset B, which is an independent subset from the Elbe and Danube regions not used in model recalibration and tuning. Most models retain stable performance, while the blending algorithm shows improved consistency and lowest error, confirming its robustness within known regional conditions.

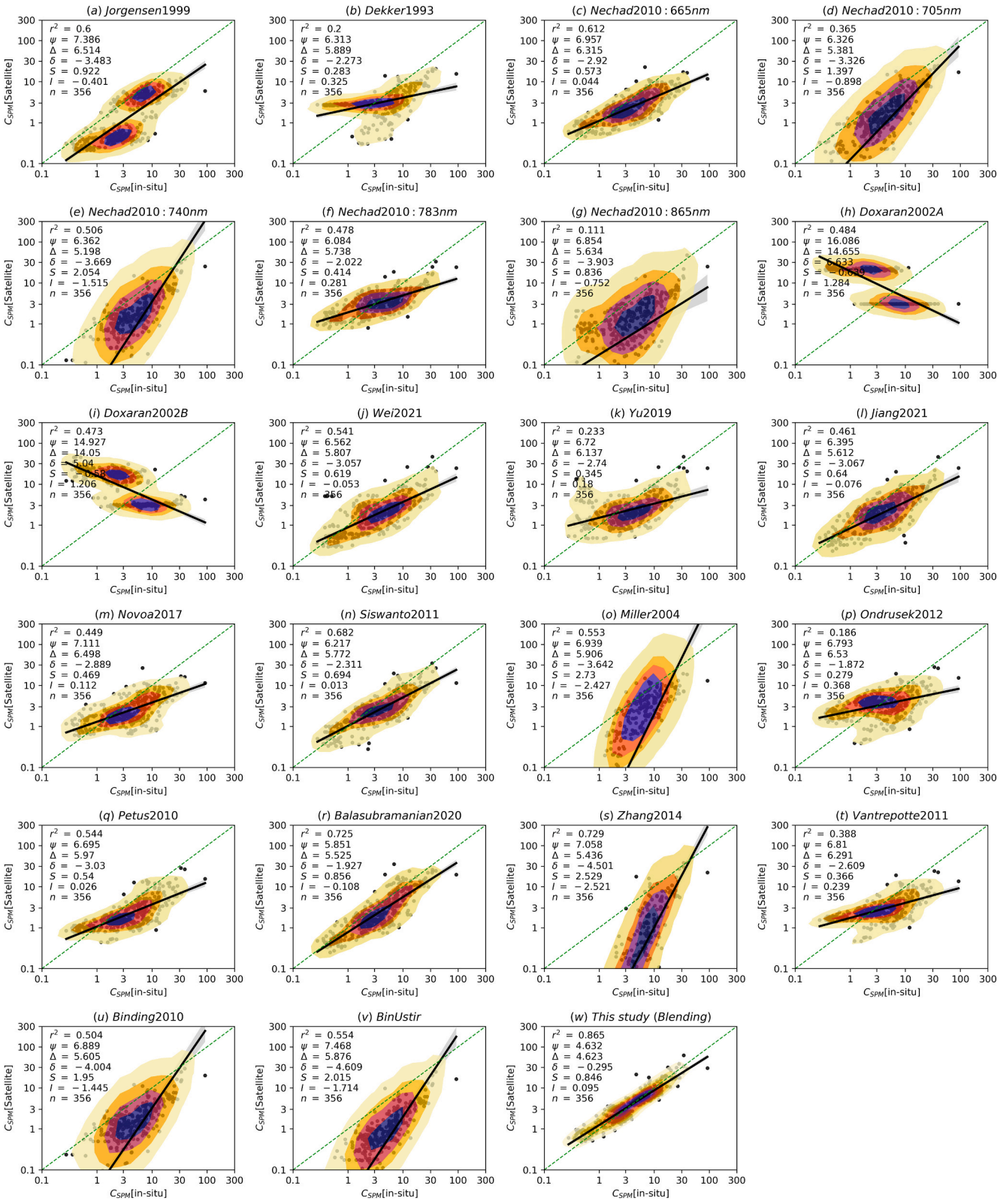

Fig. 8. External validation in new regions using Dataset C, which includes measurements from Tagus, Venice, Curonian, Black Sea, and Étang de Berre regions entirely excluded from recalibration. This evaluation highlights the challenge of model transferability. While individual models show increased scatter and underestimation, the blending algorithm maintains strong performance, demonstrating its adaptability to diverse optical environments.

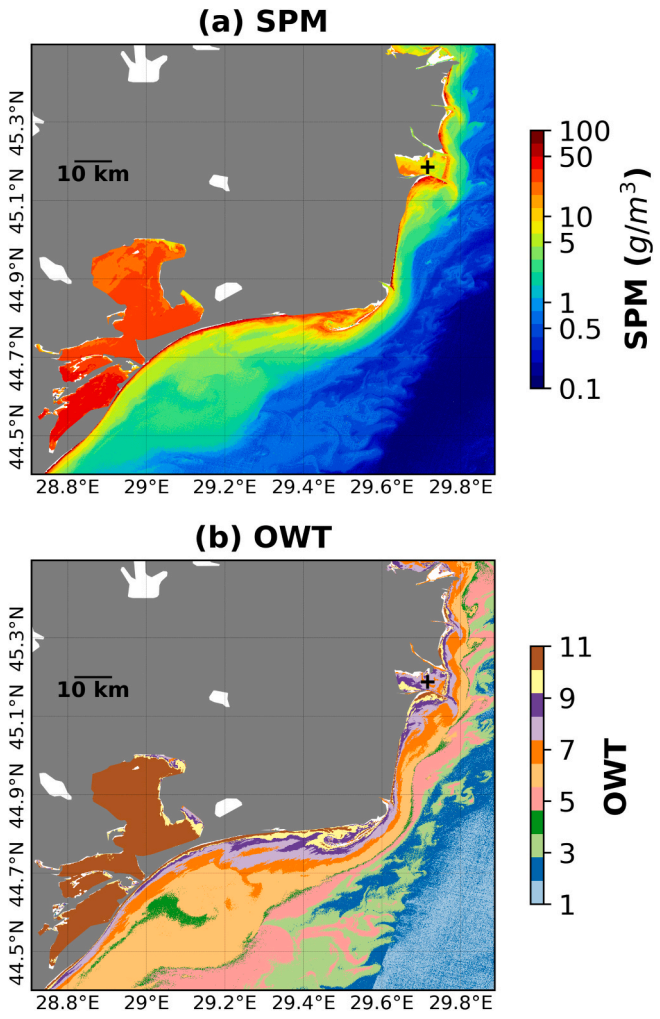

Fig. 9. Application of the SPM blending method to MSI images of the Danube coastal region on March 23, 2022: (a) SPM concentration distribution and (b) OWT classification. The black '+' indicates the location used for the analysis shown in Fig. 10.

with membership-weighted blending reduces cross-type performance variability.

5.3.4. Representativeness of calibration samples

Uncertainty also arises from the representativeness of the calibration matchups within each OWT. Because OWT classes can differ in their covered SPM ranges, spatial/temporal sampling, and underlying optical conditions, the per-OWT recalibrated coefficients may not be equally transferable when applied to independent regions or seasons. This behaviour is reflected in the OWT-stratified validation results (Supplementary Fig. S7), which show substantial variability in error magnitude (Ψ), explained variance (r^2), and bias (δ) among OWTs. These inter-class differences indicate that some optical regimes are more challenging to parameterize robustly than others under the available matchup coverage, and they motivate future efforts to broaden matchup diversity—particularly for under-represented optical regimes and extreme conditions—to further improve the stability of per-OWT recalibration and the robustness of the blended product. Consequently, improving matchup representativeness is expected to primarily reduce inter-OWT performance variability and further enhance the transferability of the OWT-guided blending framework.

5.4. Applications of the blending method in coastal monitoring

In the Danube coastal area, the method effectively identified gradients from turbid riverine inputs to clearer offshore waters (Fig. 9). This level of precision is critical for identifying areas prone to pollution or eutrophication, facilitating targeted environmental interventions. Furthermore, temporal analysis (Fig. 10) revealed seasonal fluctuations in SPM concentrations, such as increased turbidity in winter, providing insights into ecosystem dynamics and the impacts of seasonal changes on water quality. Similarly, in the Tagus-Sado region, the method successfully mapped estuarine plumes and their influence on coastal SPM distribution (Fig. 11). Its ability to resolve sharp gradients in SPM concentrations and OWTs underscores its suitability for monitoring land-sea interactions, where dynamic water properties create complex patterns. Such precision is particularly valuable for managing biodiversity-rich estuarine ecosystems, which are highly sensitive to anthropogenic pressures.

These findings underscore the broader applicability of the blending method in coastal monitoring. By providing high-resolution SPM estimates, it can enhance assessments of sediment transport, water quality, and habitat management. Given its success in two optically distinct transitional systems, the method shows clear potential for broader regional application, though global implementation will require further validation across a wider range of optical regimes.

5.5. Geographical and optical scope of applicability

The proposed framework is calibrated and evaluated using matchup data from seven European transitional/coastal regions (Elbe, Danube, Tagus, Venice, Curonian, Black Sea, and Étang de Berre), representing a broad SPM range but not necessarily the full diversity of optical conditions encountered globally. As such, the reported performance and the per-OWT optimal algorithm selections are expected to be most applicable to temperate transitional/coastal waters with optical regimes comparable to those represented in our dataset. Optical environments that are under-represented here—such as extremely turbid river plumes, tropical waters with different particulate composition, or strongly CDOM-dominated waters—may exhibit different ρ_w–SPM relationships and different distributions of OWT memberships, which could affect the membership structure and algorithm performance. While the OWT-guided recalibration and membership-weighted blending framework is generic, global application would require additional validation and, where necessary, retraining: (i) updating or extending the OWT definitions to better represent region-specific optical regimes, and/or (ii) recalibrating per-OWT algorithm coefficients using representative matchups from those regions. We therefore position the current work as a scalable framework whose robustness can be progressively improved through incorporation of additional geographically and optically diverse datasets.

5.6. Future research directions

An immediate next step for future research is the global validation of the blending method. While the approach has demonstrated robustness within the studied datasets, its applicability across a broader spectrum of water types remains untested. Systematic validation in diverse aquatic settings would refine its adaptability and contribute to the development of a universally applicable SPM estimation model. Future work could also explore whether the OWT definitions themselves should evolve with seasonal or long-term optical changes, rather than remaining fixed.

Building on this, future work should also examine the temporal dynamics of blending model performance. Seasonal shifts, episodic hydrological events, and changes in particulate composition can all influence water optical properties and thus algorithm suitability. Investigating the stability and adaptability of the blending framework under these conditions would provide insight into its long-term

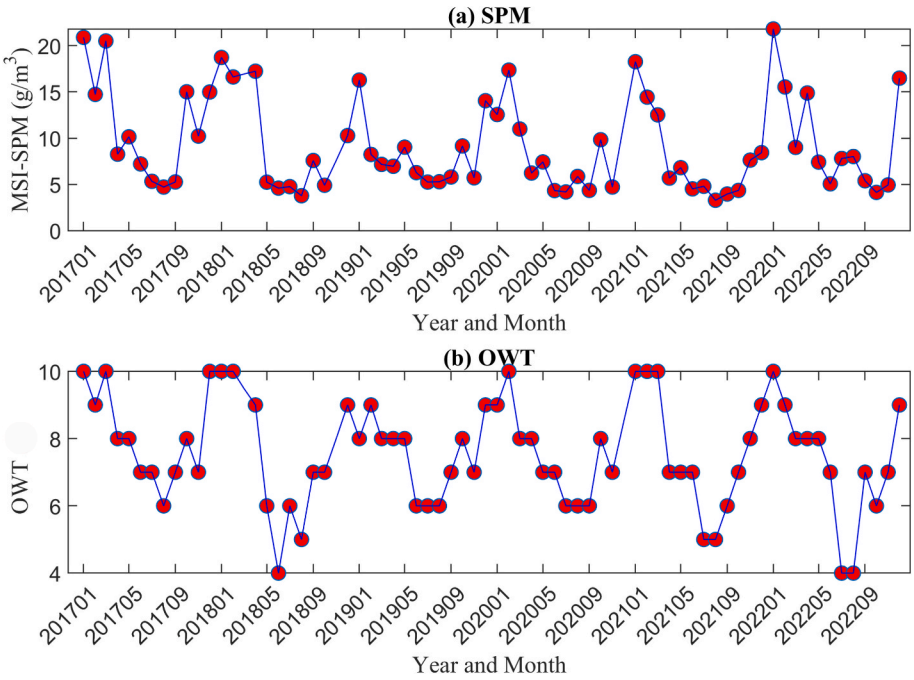

Fig. 10. Monthly time series of (a) SPM concentration and (b) OWT at a location in the Danube coastal region, denoted by a black '+' symbol in Fig. 9.

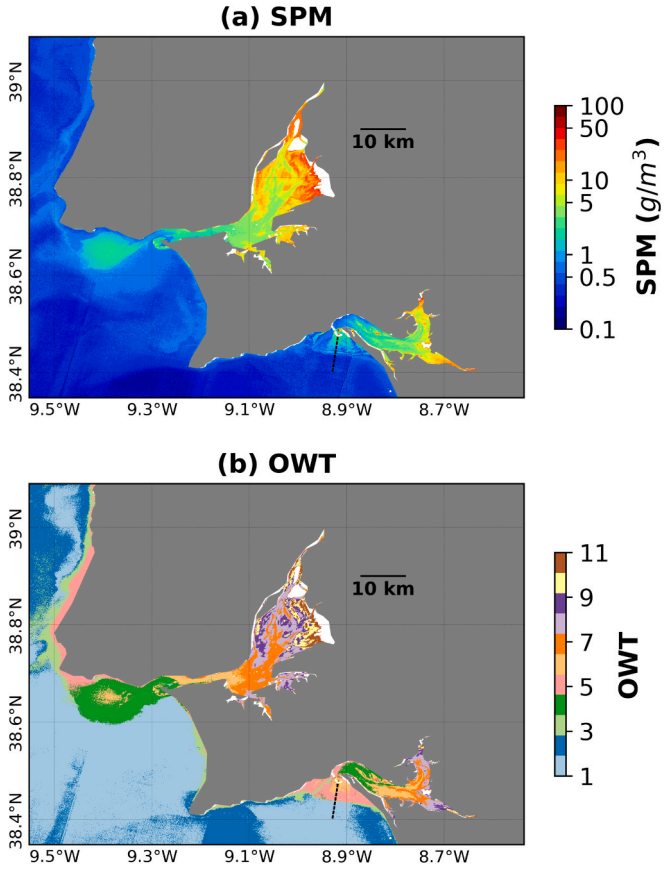

Fig. 11. Same as for Fig. 9, with another example of application in the Tagus-Sado region on April 29, 2022. Black dotted transect used for analysis in Fig. 12.

operational potential.

Finally, multi-sensor integration represents a promising direction for further enhancing the accuracy and spatial–temporal coverage of SPM retrievals. Incorporating sensors with higher spectral and spatial resolution could improve precision and provide a more detailed representation of dynamic aquatic environments, particularly in regions with complex optical properties. A multi-sensor framework would enable a more comprehensive characterization of SPM variability, improving model reliability across diverse water conditions. Integrating machine-learning architectures with OWT-based physical constraints may further enhance robustness while preserving interpretability.

6. Conclusion

In this study, we conducted an extensive evaluation of 17 SPM algorithms, utilizing an independent matchup of satellite-derived ρ_w and in-situ SPM measurements. Our findings showed that, even after careful recalibration using the matchup dataset, the performance of individual algorithms remained limited. In response to these limitations, we employed an OWT-based SPM blending methodology, designed to enhance the accuracy of SPM estimation by selecting the most appropriate SPM algorithm for each specific OWT. This selection process was carried out using a rigorous Round-Robin assessment approach. As a result, the overall SPM retrievals showed substantial improvement, with Ψ errors from 4.6 to 8.2 g/m^3 and r^2 values from 0.87 to 0.91. To demonstrate the effectiveness of this innovative blending approach, we applied it to MSI images captured in complex coastal waters, enabling us to unveil the spatial and temporal variability of SPM. The blending framework provides a robust and scalable approach for both environmental monitoring and climate-related applications, greatly enhancing our capabilities in these domains.

CRediT authorship contribution statement

Junfang Lin: Writing – review & editing, Writing – original draft, Visualization, Validation, Investigation, Formal analysis. **Elizabeth C. Atwood:** Writing – review & editing, Project administration, Funding acquisition, Data curation. **Xiaohan Liu:** Writing – review & editing. **Emmanuel Nwokocha:** Data curation. **Thomas Jackson:** Writing – review & editing. **Steve Groom:** Project administration, Funding acquisition.

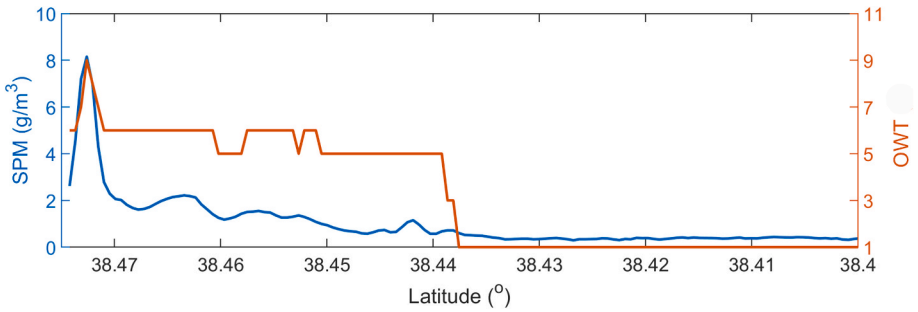

Fig. 12. SPM and OWT distributions along a transect (indicated by the black dotted line in Fig. 11) from the Sado Estuary mouth to offshore waters.

Funding

Junfang Lin, Elizabeth C. Atwood, Emmanuel Nwokocha, Thomas Jackson and Steve Groom acknowledge funding from the EC Horizon 2020 CERTO ('Copernicus Evolution: Research for harmonised and Transitional water Observation') project, grant agreement No. 870349. Junfang Lin, Elizabeth C. Atwood and Steve Groom further acknowledge funding from EC Horizon 2020 project DOORS ('Developing Optimal and Open Research Support' for the Black Sea), grant agreement No. 101000518. Elizabeth C. Atwood was partially funded by the UK Natural Environment Research Council's National Capability International programme through the FOCUS: Future states Of the global Coastal ocean: Understanding for Solutions project (project reference: NE/X006271/1). Steve Groom was partially funded by UK Natural Environment Research Council (NERC) through the NERC Earth Observation Data Analysis and Artificial Intelligence Service (NEODAAS), overseen by the National Centre for Earth Observation (NCEO).

Declaration of competing interest

The authors declare that they have no known competing financial interests or personal relationships that could have appeared to influence the work reported in this paper.

Acknowledgments

The authors would like to extend their thanks for the support by the wider CERTO consortium through provision of ideas and data to support development and analyses. In particular, the authors would like to recognize the extensive efforts by the field teams for the in-situ data collected at each of the six CERTO study sites. These concerted campaigns were led and/or executed by: Victor Martinez Vicente (PML) for the Plymouth Sound/Tamar Estuary; Vanda Brotas, Ana Brito and Giulia Sent (University of Lisbon) for the Tagus Estuary; Federica Braga (CNR) for the Venice Lagoon; Mariano Bresciani (CNR) and Diana Vaiciute (Klaipėda University) for the Curonian Lagoon; Adriana Maria Constantinescu (GeoEcoMar) for the Razelm-Sinoe Lagoon system; Carole Lebreton (Brockmann Consulting GmbH) and Rüdiger Röttgers (HEREON) for the Elbe River and German Bight. Field sampling efforts across the CERTO sites were consistently supported by the dedicated team at the University of Stirling, whom the authors would especially like to acknowledge: Dalin Jiang, Evangelos Spyrakos, Veloisa Mascarenhas, and Andrew Tyler. We also acknowledge the LIMNADES initiative, as well as the many data providers whose in-situ measurements enabled this study (in particular, the DOORS cruises 1-3 field sampling teams headed by Violeta Slabakova at the Institute of Oceanology, Bulgarian Academy of Sciences, with support by Dalin Jiang).

Appendix A. Supplementary data

Supplementary data to this article can be found online at https://doi.org/10.1016/j.jag.2026.105302.

Data availability

The Black Sea cruise datasets used in this study are publicly available via Zenodo at: https://doi.org/10.5281/zenodo.15120079, https://doi.org/10.5281/zenodo.15119521, and https://doi.org/10.5281/zenodo.14978829. The remaining datasets are available from the corresponding author upon reasonable request and are subject to project and data provider agreements.

References

Atwood, E.C., Jackson, T., Laurenson, A., Jönsson, B.F., Spyrakos, E., Jiang, D., Sent, G., Selmes, N., Simis, S., Danne, O., 2024. Framework for regional to global extension of optical water types for remote sensing of optically complex transitional water bodies. Remote Sens. (Basel) 16, 3267. https://doi.org/10.3390/rs16173267.

Balasubramanian, S.V., Pahlevan, N., Smith, B., Binding, C., Schalles, J., Loisel, H., Gurlin, D., Greb, S., Alikas, K., Randla, M., 2020. Robust algorithm for estimating total suspended solids (TSS) in inland and nearshore coastal waters. Remote Sens. Environ. 246, 111768. https://doi.org/10.1016/j.rse.2020.111768.

Binding, C., Jerome, J., Bukata, R., Booty, W., 2010. Suspended particulate matter in Lake Erie derived from MODIS aquatic colour imagery. Int. J. Remote Sens. 31, 5239–5255. https://doi.org/10.1080/01431160903302973.

Brewin, R.J., Sathyendranath, S., Müller, D., Brockmann, C., Deschamps, P.-Y., Devred, E., Doerffer, R., Fomferra, N., Franz, B., Grant, M., 2015. The Ocean Colour Climate Change Initiative: III. A round-robin comparison on in-water bio-optical algorithms. Remote Sens. Environ. 162, 271–294. https://doi.org/10.1016/j.rse.2013.09.016.

Cox, C., Munk, W., 1954. Measurement of the roughness of the sea surface from photographs of the sun's glitter. J. Opt. Soc. Am. 44, 838–850. https://doi.org/10.1364/JOSA.44.000838.

Dekker, A.G., 1993. Detection of optical water quality parameters for eutrophic waters by high resolution remote sensing. Vrije Universiteit Amsterdam, Amsterdam, The Netherlands. PhD thesis.

Doxaran, D., Froidefond, J.-M., Lavender, S., Castaing, P., 2002. Spectral signature of highly turbid waters: Application with SPOT data to quantify suspended particulate matter concentrations. Remote Sens. Environ. 81, 149–161. https://doi.org/10.1016/S0034-4257(01)00341-8.

Jackson, T., Sathyendranath, S., Mélin, F., 2017. An improved optical classification scheme for the Ocean Colour Essential Climate Variable and its applications. Remote Sens. Environ. 203, 152–161. https://doi.org/10.1016/j.rse.2017.03.036.

Jiang, D., Matsushita, B., Pahlevan, N., Gurlin, D., Lehmann, M.K., Fichot, C.G., Schalles, J., Loisel, H., Binding, C., Zhang, Y., 2021. Remotely estimating total suspended solids concentration in clear to extremely turbid waters using a novel semi-analytical method. Remote Sens. Environ. 258, 112386. https://doi.org/10.1016/j.rse.2021.112386.

Jorgensen, P.V., 1999. Standard CZCS Case 1 algorithms in danish coastal waters. Int. J. Remote Sens. 20, 1289–1301. https://doi.org/10.1080/014311699212731.

Liu, X., Steele, C., Simis, S., Warren, M., Tyler, A., Spyrakos, E., Selmes, N., Hunter, P., 2021. Retrieval of Chlorophyll-a concentration and associated product uncertainty in optically diverse lakes and reservoirs. Remote Sens. Environ. 267, 112710. https://doi.org/10.1016/j.rse.2021.112710.

Manivanan, R., 2008. Water Quality Modeling: Rivers, Streams, and Estuaries. New India Publishing, New Delhi.

Martin, S., Bryère, P., Gernez, P., Renosh, P.R., Doxaran, D., 2025. Towards Reliable High-Resolution Satellite Products for the monitoring of Chlorophyll-a and Suspended Particulate Matter in Optically Shallow Coastal Lagoons. Remote Sens. (Basel) 17, 3430. https://doi.org/10.3390/rs17203430.

Matthews, M.W., 2011. A current review of empirical procedures of remote sensing in inland and near-coastal transitional waters. Int. J. Remote Sens. 32, 6855–6899. https://doi.org/10.1080/01431161.2010.512947.

Miller, R.L., McKee, B.A., 2004. Using MODIS Terra 250 m imagery to map concentrations of total suspended matter in coastal waters. Remote Sens. Environ. 93, 259–266. https://doi.org/10.1016/j.rse.2004.07.012.

Moore, T.S., Campbell, J.W., Dowell, M.D., 2009. A class-based approach to characterizing and mapping the uncertainty of the MODIS ocean chlorophyll

product. Remote Sens. Environ. 113, 2424–2430. https://doi.org/10.1016/j.rse.2009.07.016.
Moore, T.S., Campbell, J.W., Feng, H., 2001. A fuzzy logic classification scheme for selecting and blending satellite ocean color algorithms. IEEE Trans. Geosci. Remote Sens. 39, 1764–1776. https://doi.org/10.1109/36.942555.
Nechad, B., Ruddick, K.G., Park, Y., 2010. Calibration and validation of a generic multisensor algorithm for mapping of total suspended matter in turbid waters. Remote Sens. Environ. 114, 854–866. https://doi.org/10.1016/j.rse.2009.11.022.
Neil, C., Spyrakos, E., Hunter, P.D., Tyler, A.N., 2019. A global approach for chlorophyll-a retrieval across optically complex inland waters based on optical water types. Remote Sens. Environ. 229, 159–178. https://doi.org/10.1016/j.rse.2019.04.027.
Neukermans, G., Loisel, H., Mériaux, X., Astoreca, R., McKee, D., 2012. In situ variability of mass-specific beam attenuation and backscattering of marine particles with respect to particle size, density, and composition. Limnol. Oceanogr. 57, 124–144. https://doi.org/10.4319/lo.2012.57.1.0124.
Novoa, S., Doxaran, D., Ody, A., Vanhellemont, Q., Lafon, V., Lubac, B., Gernez, P., 2017. Atmospheric corrections and multi-conditional algorithm for multi-sensor remote sensing of suspended particulate matter in low-to-high turbidity levels coastal waters. Remote Sens. (Basel) 9, 61. https://doi.org/10.3390/rs9010061.
Odermatt, D., Gitelson, A., Brando, V.E., Schaepman, M., 2012. Review of constituent retrieval in optically deep and complex waters from satellite imagery. Remote Sens. Environ. 118, 116–126. https://doi.org/10.1016/j.rse.2011.11.013.
Ondrusek, M., Stengel, E., Kinkade, C.S., Vogel, R.L., Keegstra, P., Hunter, C., Kim, C., 2012. The development of a new optical total suspended matter algorithm for the Chesapeake Bay. Remote Sens. Environ. 119, 243–254. https://doi.org/10.1016/j.rse.2011.12.018.
Petus, C., Chust, G., Gohin, F., Doxaran, D., Froidefond, J.-M., Sagarminaga, Y., 2010. Estimating turbidity and total suspended matter in the Adour River plume (South Bay of Biscay) using MODIS 250-m imagery. Cont. Shelf Res. 30, 379–392. https://doi.org/10.1016/j.csr.2009.12.007.
Sent, G., Antunes, C., Spyrakos, E., Jackson, T., Atwood, E.C., Brito, A.C., 2025. What time is the tide? The importance of tides for ocean colour applications to estuaries. Remote Sens. Appl.: Soc. Environ. 37, 101425. https://doi.org/10.1016/j.rsase.2024.101425.
Siswanto, E., Tang, J., Yamaguchi, H., Ahn, Y.-H., Ishizaka, J., Yoo, S., Kim, S.-W., Kiyomoto, Y., Yamada, K., Chiang, C., 2011. Empirical ocean-color algorithms to retrieve chlorophyll-a, total suspended matter, and colored dissolved organic matter absorption coefficient in the Yellow and East China Seas. J. Oceanogr. 67, 627–650. https://doi.org/10.1007/s10872-011-0062-z.
Spyrakos, E., O'Donnell, R., Hunter, P.D., Miller, C., Scott, M., Simis, S.G., Neil, C., Barbosa, C.C., Binding, C.E., Bradt, S., 2018. Optical types of inland and coastal waters. Limnol. Oceanogr. 63, 846–870. https://doi.org/10.1002/lno.10674.
Strickland, J.D.H., Parsons, T.R., 1972. A Practical Handbook of Seawater Analysis, 2nd ed. Fisheries Research Board of Canada, Ottawa, Bulletin, p. 167.
Tavora, J., Boss, E., Doxaran, D., Hill, P., 2020. An algorithm to estimate suspended particulate matter concentrations and associated uncertainties from remote sensing reflectance in coastal environments. Remote Sens. (Basel) 12, 2172. https://doi.org/10.3390/rs12132172.
Turner, A., Millward, G., 2002. Suspended particles: their role in estuarine biogeochemical cycles. Estuar. Coast. Shelf Sci. 55, 857–883. https://doi.org/10.1006/ecss.2002.1033.
Uudeberg, K., Ansko, I., Põru, G., Ansper, A., Reinart, A., 2019. Using optical water types to monitor changes in optically complex inland and coastal waters. Remote Sens. (Basel) 11, 2297. https://doi.org/10.3390/rs11192297.
Vanhellemont, Q., Ruddick, K., 2018. Atmospheric correction of metre-scale optical satellite data for inland and coastal water applications. Remote Sens. Environ. 216, 586–597. https://doi.org/10.1016/j.rse.2018.07.015.
Vantrepotte, V., Loisel, H., Mériaux, X., Neukermans, G., Dessailly, D., Jamet, C., Gensac, E., Gardel, A., 2011. Seasonal and inter-annual (2002-2010) variability of the suspended particulate matter as retrieved from satellite ocean color sensor over the French Guiana coastal waters. J. Coast. Res. SI 64, 1750–1754.
Wei, J., Wang, M., Jiang, L., Yu, X., Mikelsons, K., Shen, F., 2021. Global estimation of suspended particulate matter from satellite ocean color imagery. J. Geophys. Res. Oceans 126, e2021JC017303. https://doi.org/10.1029/2021JC017303.
Wolanski, E., Elliott, M., 2015. Estuarine ecohydrology: an Introduction, 2nd ed. Elsevier, Amsterdam.
Yu, X., Lee, Z., Shen, F., Wang, M., Wei, J., Jiang, L., Shang, Z., 2019. An empirical algorithm to seamlessly retrieve the concentration of suspended particulate matter from water color across ocean to turbid river mouths. Remote Sens. Environ. 235, 111491. https://doi.org/10.1016/j.rse.2019.111491.
Zhang, Y., Shi, K., Liu, X., Zhou, Y., Qin, B., 2014. Lake topography and wind waves determining seasonal-spatial dynamics of total suspended matter in turbid Lake Taihu, China: assessment using long-term high-resolution MERIS data. PLoS One 9, e98055. https://doi.org/10.1371/journal.pone.0098055.